Comparative Medicine
Copyright 2016
by the American Association for Laboratory Animal Science

Vol 66, No 4
August 2016
Pages 268–277

*Original Research*

# Echocardiographic Characterization of a Murine Model of Hypertrophic Obstructive Cardiomyopathy Induced by Cardiac-specific Overexpression of Epidermal Growth Factor Receptor 2

**Lars L Sørensen,[1,3] Djahida Bedja,[2] Polina Sysa-Shah,[2] Hongyun Liu,[1] Amanda Maxwell,[2] Xu Yi,[2] Iraklis Pozios,[1] Niels T Olsen,[4] Theodore P Abraham,[1] Roselle Abraham,[1] and Kathleen Gabrielson[2,*]**

**Although rare, hypertrophic cardiomyopathy (HCM) with midventricular obstruction is often associated with severe symptoms and complications. None of the existing HCM animal models display this particular phenotype. Our group developed a mouse line that overexpresses the ErbB2 receptor (ErbB2$^{tg}$) in cardiomyocytes; we previously showed that the ErbB2 receptor induces cardiomyocyte hypertrophy, myocyte disarray, and fibrosis compatible with HCM. In the current study, we sought to further echocardiographically characterize the ErbB2$^{tg}$ mouse line as a model of HCM. Compared with their wild-type littermates, ErbB2$^{tg}$ mice show increased left ventricular (LV) mass, concentric LV hypertrophy, and papillary muscle hypertrophy. This hypertrophy was accompanied by diastolic dysfunction, expressed as reduced E:A ratio, prolonged deceleration time, and elevated E:e′ ratio. In addition, ErbB2$^{tg}$ mice consistently showed midcavity obstruction with elevated LV gradients, and the flow profile revealed a prolonged pressure increase and a delayed peak, indicating dynamic obstruction. The ejection fraction was increased in ErbB2$^{tg}$ mice, due to reduced end-diastolic and end-systolic LV volumes. Furthermore, systolic radial strain and systolic radial strain rate but not systolic circumferential strain and longitudinal strain were decreased in ErbB2$^{tg}$ compared with wild-type mice. In conclusion, the phenotype of the ErbB2$^{tg}$ mouse model is consistent with midventricular HCM in many important aspects, including massive LV hypertrophy, diastolic dysfunction, and midcavity obstruction. This pattern is unique for a small animal model, suggesting that ErbB2$^{tg}$ mice may be well suited for research into the hemodynamics and treatment of this rare form of HCM.**

**Abbreviations:** ErbB2, cardiac-specific epidermal growth factor receptor 2; HCM, hypertrophic cardiomyopathy; LV, left ventricle; LVAW, LV anterior wall thickness; LVIDD, LV internal diastolic diameter; LVPW, LV posterior wall thickness; TDI, tissue Doppler imaging

Hypertrophic cardiomyopathy (HCM) is the most commonly inherited cardiac disease, is caused by mutations in the genes that encode sarcomere proteins, is characterized by hypertrophy of the left ventricle, and affects 1 in 500 persons. More than 900 known mutations affect 20 genes, but the mutations involving cardiac muscle β-myosin heavy chain, cardiac myosin-binding protein C, and cardiac muscle troponin T account for the majority of cases of HCM with a known mutation. However, 60% of patients with clinical HCM without family history and 30% of patients with family history of HCM have no known mutation.[8] Therefore, the cause underlying HCM in a substantial number of patients is unknown. HCM has a diverse clinical and morphologic presentation. Classic HCM is characterized by left ventricular (LV) hypertrophy, diastolic dysfunction, and LV obstruction localized to the LV outflow tract and caused by systolic anterior movement of the mitral valve.[9] However some patients present with midventricular hypertrophy and midcavity obstruction due to papillary muscle hypertrophy or cavity obliteration.[7,18] These patients can have severe symptoms, develop apical aneurysms, and often need surgical myectomy (Figure 1).[7]

Several mouse models of HCM based on documented human mutations have been created, both representing the common mutations in β-myosin heavy chain and troponin T as well as for rarer mutations.[2,12,19,32] These mouse models have given great insight into the pathogenesis and cellular disturbances of HCM, but the available models typically present a mild phenotype with no or mild to moderate hypertrophy and mild diastolic dysfunction, and none of the existing models develop LV obstruction.[2,19,32] Even the mouse model based on a mutation known to produce midventricular obstructive HCM in humans doesn't display a

*Received: 16 Sep 2015. Revision requested: 26 Oct 2015. Accepted: 01 Feb 2016.*
*[1]Department of Cardiology and [2]Department of Molecular and Comparative Pathobiology, School of Medicine, Johns Hopkins University, Baltimore, Maryland; [3]Department of Cardiology, Gentofte Hospital, Copenhagen, Denmark; and [4]Department of Cardiology, Rigshospitalet, Copenhagen, Denmark.*
**Corresponding author. Email:kgabriel@jhmi.edu*

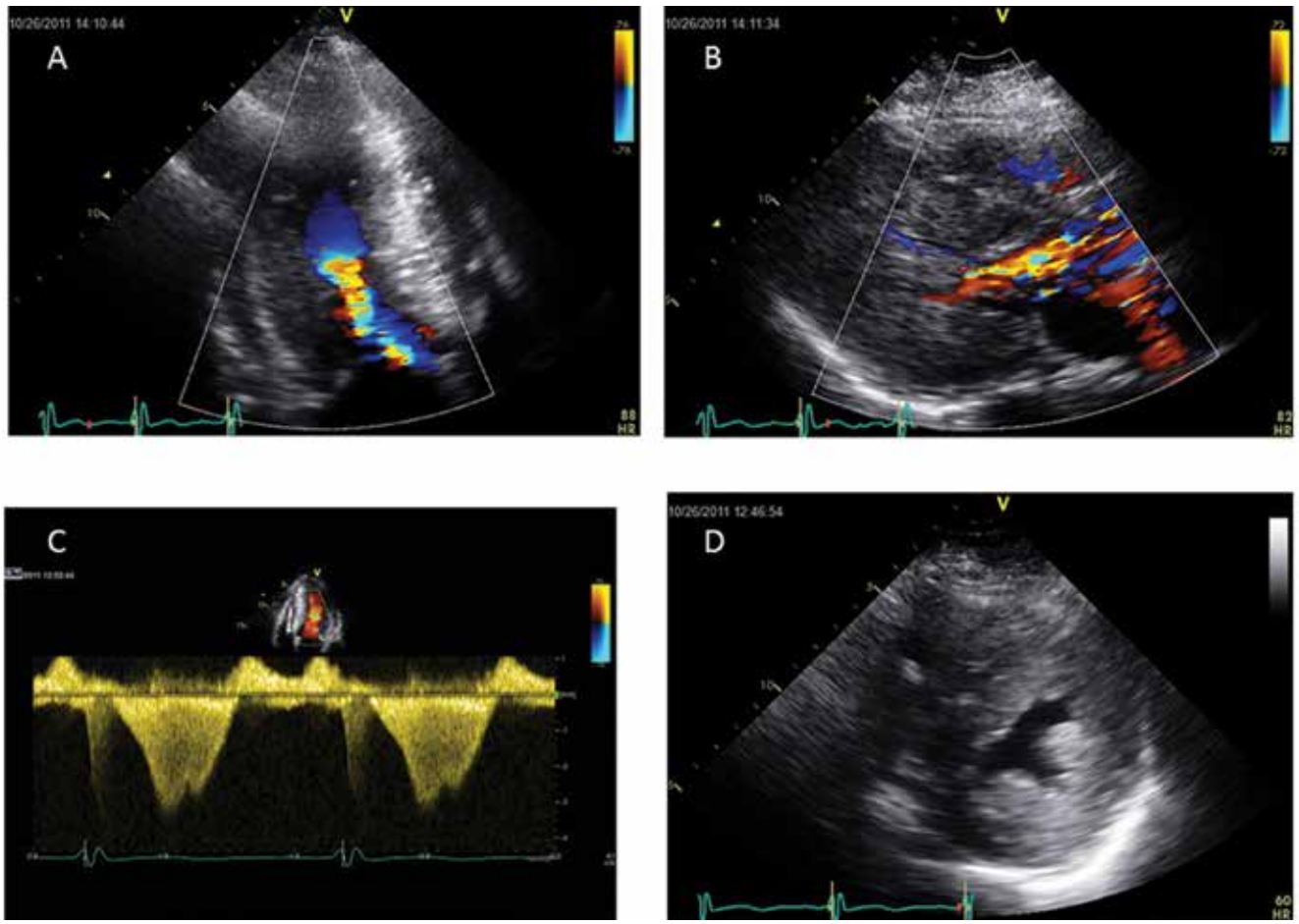


**Figure 1.** Midventricular obstructive hypertrophic cardiomyopathy in humans. (A and B) Color Doppler images showing left midventricular obstruction and turbulent flow, caused by contact between the hypertrophied septum and papillary muscle. (C) Continuous-wave Doppler measurement of increased midventricular gradient (65 mm Hg). (D) Short-axis view showing concentric left-ventricular hypertrophy and papillary muscle hypertrophy. All images are from the same patient.

phenotype with LV obstruction.[12] Therefore, additional animal models with morphologic features similar to human HCM should be characterized to uncover pathways that could be potentially involved in this genetically heterogeneous disease.

Our group has developed a mouse model characterized by overexpression of cardiac-specific epidermal growth factor receptor 2 overexpression (ErbB2$^{tg}$ mice).[30] These mice have fetal gene expression that is associated with cardiac hypertrophy and increased activity of prosurvival and hypertrophic pathways including the PI3K–AKT pathway. However, one particularly interesting and unexpected feature of the ErbB2$^{tg}$ mouse is the marked LV hypertrophy with histologic features compatible with HCM, including myocyte disarray, fibrosis, and myocyte hypertrophy.[30] Electrocardiographic characterization of these mice revealed distinct ECG changes and repolarization abnormalities compatible with HCM.[29] In the current study, we further characterized this transgenic mouse as a potential model of HCM by performing a thorough echocardiographic evaluation of LV morphology, hemodynamics, and diastolic and systolic function with correlations to gross pathology.

## Materials and Methods

**Transgenic constructs and mouse lines.** The transgenic mice were constructed as described earlier.[30] Briefly, rat ErbB2 mRNA was isolated and converted to cDNA. The 5-Kb cDNA fragment was then subcloned into the *Bam*HI–*Sal*I site of the cardiac-specific expression vector, α-myosin heavy-chain promoter construct (kindly provided by Dr Jeffrey Robbins), followed by the polyadenylation signal from human growth hormone, located downstream of the insert. The B6SJLF1/J mouse strain was used for pronuclear microinjection of the received fragment and production of the transgenic mice by Johns Hopkins Transgenic Core Facility. Founder animals were identified by PCR and Southern blot analysis. Two founders were used to develop 2 independent transgenic lines, which have the same phenotype.

**Animals.** This study was performed in strict accordance with the recommendations in the *Guide for the Care and Use of Laboratory Animals*[11] of the NIH. The protocol was approved by the Committee on the Ethics of Animal Experiments of the Johns Hopkins Medical Institutions (Animal Welfare Assurance no. A-3273-01). All of the transgenic mice and wild-type littermates (line 6) used for these studies were housed in top-ventilated cages under a 12:12-h light:dark cycle with free access to food and water, temperature at 72 °F (22 °C), and humidity at 42%. Mice were negative for fur mites, pinworms, *Helicobacter* spp., mouse hepatitis virus, epidemic diarrhea of infant mice virus (rotavirus), minute virus of mice, mouse parvovirus types 1 and 2, mouse theilovirus,

mouse adenovirus types 1 and 2, ectromelia virus, lymphocytic choriomeningitis virus, *Mycoplasma pulmonis*, pneumonia virus of mice, reovirus, Sendai virus, mouse norovirus, and mouse cytomegalovirus. Mice were euthanized by using $CO_2$, according to the AVMA guidelines and Johns Hopkins University Animal Care and Use Committee Guidelines for Euthanasia of Rats and Mice Using Carbon Dioxide (July 2008).

**Echocardiography.** In vivo cardiac morphology and function were assessed by using a high-frequency, high-resolution echocardiography system consisting of a Vevo 2100 ultrasound machine equipped with a 40-MHz transducer (Visual Sonics, Toronto, Canada). The mice were examined as described earlier.[2] Briefly, mice were imaged under light anesthesia with 1% to 2% isoflurane, positioned on a heated imaging platform with built-in electrocardiography and thermometer to continuously monitor heart rate and temperature. Body temperature was maintained at 37 °C. The examination typically took a total of 25 min: induction of anesthesia and stabilization of heart rate took around 10 min, and the echocardiography examination required 15 min. The mouse typically recovered in 1 to 2 min after the termination of anesthesia. We evaluated systolic and diastolic function with conventional M-mode and 2D echocardiography supplemented by color Doppler, pulse-wave Doppler, tissue Doppler imaging (TDI), and deformation analysis by 2D speckle tracking. All echocardiography and image analysis was done by a single investigator (LLS), who was blinded to mouse genotype. Intraobserver variability was assessed for a single investigator (HL).

***Conventional echocardiography.*** Wall thickness and LV dimensions were measured along the short axis at papillary muscle level by using M-mode images.[31] The following parameters were measured: LV anterior wall thickness (LVAW); LV posterior wall thickness (LVPW); LV internal diastolic diameter (LVIDD); and LV internal systolic diameter (LVIDS). LV mass was calculated using the following formula (LV mass = $1.053 \times [(\text{LVIDD} + \text{LVPW} + \text{LVAW})^3 - \text{LVIDD}^3]$. LV volumes were obtained by direct planimetry of the LV wall contour in the long-axis view to get a volume in end-diastole and end-systole. We also assessed LV volume and geometry by comparison of LVIDD and LVIDS in the short-axis view. The LV ejection fraction was calculated from the LV volumes and expressed as a percentage.[4]

***Pulse-wave and tissue Doppler echocardiography.*** Transmitral inflow velocities were measured in the apical 4-chamber image with the pulse-wave Doppler sample placed at the tip of the mitral leaflet and guided by color Doppler images. Early (E) and late (A) diastolic velocities and deceleration time were measured.[2] TDI velocities were measured in the apical 4-chamber image with the sample placed at the mitral annulus. Systolic tissue velocity (s'), early diastolic tissue velocity (e'), and late diastolic velocity (a') were measured from these images.[26] We used the built-in angle correction to correct any problems with aligning the echo probe with the blood flow (pulse-wave Doppler) or tissue movement (TDI). Global diastolic function was assessed by E:A ratio, deceleration time, e', and E:e' ratio.[2,24,26] In addition, the fusion of the E and A waves was registered; when accompanied by fusion of e' and a', these features of are likely indicators of diastolic dysfunction.[34] Animals with fusion of E and A were excluded from analysis of E/A-ratio and deceleration time. Systolic function by TDI was evaluated by s'. Both E:e' ratio and s' are parameters often evaluated in humans but are novel in the evaluation of mice.[1] Left ventricular outflow tract gradients were measured by using pulse-wave Doppler in the apical 3-chamber image with the sample placed in the LV outflow tract and guided by the 2D and color Doppler images. In addition, the shape of the flow curve was registered to differentiate between fixed and dynamic LV obstruction.[9]

***Deformation analysis.*** Deformation analysis based on speckle tracking was performed offline using the VevoStrain 2D speckle tracking software and 300 frame loops were recorded. Analysis was done on 3 consecutive cardiac cycles with a frame rate of 279 to 309/s in long axis and 346 to 466/s in short axis. The endocardial border of the left ventricle was traced manually from a still frame image and automatically tracked throughout the cardiac cycle by the software. In the short-axis view, we measured the following global systolic and diastolic parameters: systolic circumferential strain, systolic circumferential strain rate, diastolic circumferential strain rate, systolic radial strain, systolic radial strain rate, and diastolic radial strain rate. Systolic longitudinal strain, systolic longitudinal strain rate, and diastolic longitudinal strain rate were measured in long axis, but because of poor image quality in the transgenic animals, only a subset of the animals was analyzed (5 transgenic and 6 controls). All measurements of strain and strain rate were used in the assessment of systolic- and diastolic function.[1,4]

**Pathologic examination of papillary muscles.** Male ErbB2 transgenic and wild-type littermate mice (age, 7 wk) were anesthetized by using intraperitoneal injection of ketamine (120 mg/kg) and xylazine (10 mg/kg). Mice also received intraperitoneal injections of heparin (5000 U/mL, 0.1 mL). Laparotomy was performed, the thorax opened, and a 27-gauge butterfly catheter placed in the LV apex. The intravascular pressure was released by piercing the right atrium with a 21-gauge needle. At a rate of 2 mL/min, 10 mL of PBS containing heparin (5000 U/mL) was injected into the heart and quickly followed by 5 mL of a potassium–cadmium chloride solution (0.33 M KCl, 62.7 mM $CdCl_2$, 33.3 mM Tris) to arrest the heart in diastole. Cardiac arrest was followed by perfusion with buffered formalin at 10 mL/s.[14] The heart was removed from the chest, weighed, and placed in formalin for 24 h and then ethanol for 24 h. By using a dissecting microscope, the hearts were transversely sectioned in half and the anterior and posterior aspects noted. After processing, the heart sections were embedded so that sectioning was consistent among all hearts. Hearts were sectioned at 7 µm and stained with hematoxylin and eosin (Figure 2) .

To quantify the area of the left ventricle papillary muscles, representative heart sections were compared by using NIS-Elements software (version 4.3, Nikon, Tokyo, Japan). The LV posterior and anterior papillary muscles were imaged and measured by outlining their perimeter and quantifying the area (in $mm^2$). To prepare representative figures for comparison of subgross pathology between wild-type and ErbB2 transgenic hearts, cross-sections were photographed at 4× magnification (Ci-L microscope, Nikon; DS-Ri2 16.25-MP camera system, Nikon), and images were stitched together (NIS-Elements Software version 4.3, Nikon).

**Dissection of papillary muscles.** The mice were euthanized by using intraperitoneal injections of ketamine (120 mg/kg) and xylazine (10 mg/kg), weighed, and their tibial lengths measured. The hearts were excised, sectioned in cold PBS, and the LV opened to expose the papillary muscles. Both anterior and posterior papillary muscles were dissected under a stereomicroscope by using iris scissors, weighed, and photographed.

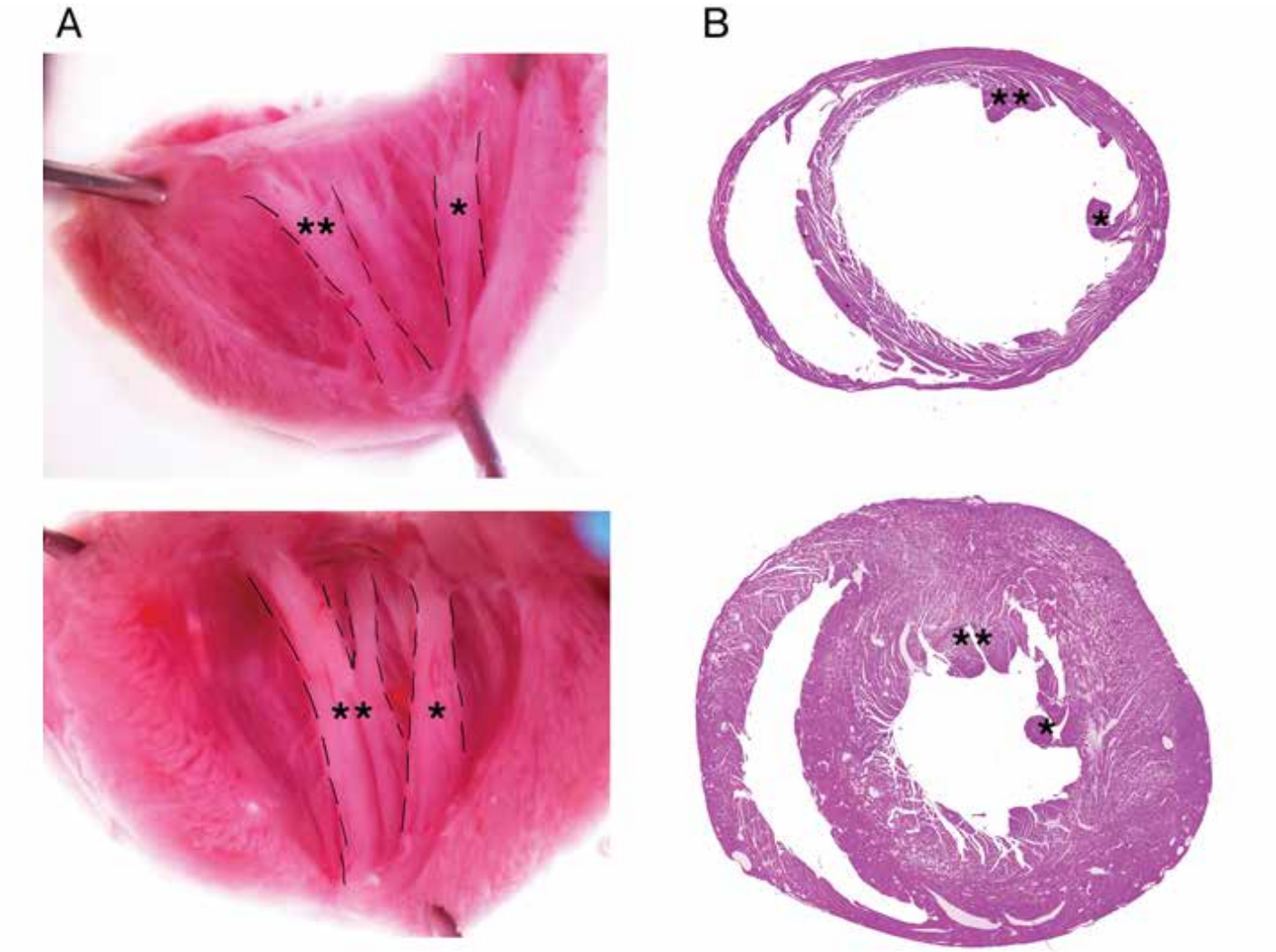


**Figure 2.** ErbB2$^{tg}$ mice show left-ventricular and papillary muscle hypertrophy. (A) Image showing resection of the papillary muscles in a wild-type mouse (top) and an ErbB2$^{tg}$ mouse (bottom), illustrating papillary muscle hypertrophy. (B) Cross-sectional pathology images showing left-ventricular and papillary muscles in a wild-type mouse (top) and an ErbB2$^{tg}$ mouse (below). *, Anterior papillary muscle; **, posterior papillary muscle.

**Statistics.** All continuous data were summarized as mean ± 1 SD. Unpaired *t* tests were used to compare continuous variables between the 2 groups. All statistical analysis was performed with Stata/IC 12.1 statistical software (StataCorp, College Station, TX). Intraobserver variability was expressed as relative values (percentage).[5]

## Results

ErbB2$^{tg}$ mice and their wild-type littermates were comparable with regard to age (50 ± 7 d compared with 48 ± 8 d, $P = 0.59$), weight (19 ± 2 g compared with 18 ± 2 g, $P = 0.47$), and heart rate (449 ± 41 bpm compared with 462 ± 44 bpm, $P = 0.42$). LVAW and LVPW were significantly greater in ErbB2$^{tg}$ mice compared with wild-type littermates (LVAW, 1.21 ± 0.20 mm compared with 0.72 ± 0.08mm, $P < 0.0001$; LVPW, 1.65 ± 0.29 mm compared with 0.75 ± 0.09 mm, $P < 0.0001$; Figures 2 and 3) . Correspondingly, LV mass was significantly greater in ErbB2$^{tg}$ than wild-type mice (220 ± 51 mg compared with 87 ± 19 mg, $P < 0.0001$).

**Papillary muscles.** Cross sections of the papillary muscles on echocardiography and after necropsy are shown in Figure 2 and 3. We compared the cross-sectional area of 4 ErbB2$^{tg}$ and 5 wild-type mice by using pathology images (Figure 2). The area of the papillary muscles was significantly greater in ErbB2$^{tg}$ mice than in wild-type animals overall (1.18 ± 0.29 mm$^2$ compared with 0.48 ± 0.06 mm$^2$, $P = 0.01$) and specifically for the anterior papillary muscle (0.32 ± 0.06 mm$^2$ compared with 0.21 ± 0.04 mm$^2$, $P = 0.02$) and posterior papillary muscle (0.86 ± 0.31 mm$^2$ compared with 0.27 ± 0.05 mm$^2$, $P = 0.03$).

We then dissected the cardiac papillary muscles of 5 ErbB2$^{tg}$ and 5 wild-type mice. The weight of both papillary muscles combined was significantly greater in the ErbB2$^{tg}$ mice than wild-type littermates (4.0 ± 0.2 mg compared with 2.6 ± 0.3 mg, $P = 0.007$), driven by the increased weight of the posterior papillary muscle (2.8 ± 0.3 mg compared with 1.6 ± 0.4 mg, $P = 0.002$), whereas weight of the anterior papillary muscle did not differ (1.3 ± 0.3 mg compared with 1.0 ± 0.3 mg, $P = 0.18$).

**Systolic function.** The comparison of markers of systolic function is summarized in Table 1. Ejection fraction was higher in ErbB2$^{tg}$ mice compared with wild-type littermates and LV vol-

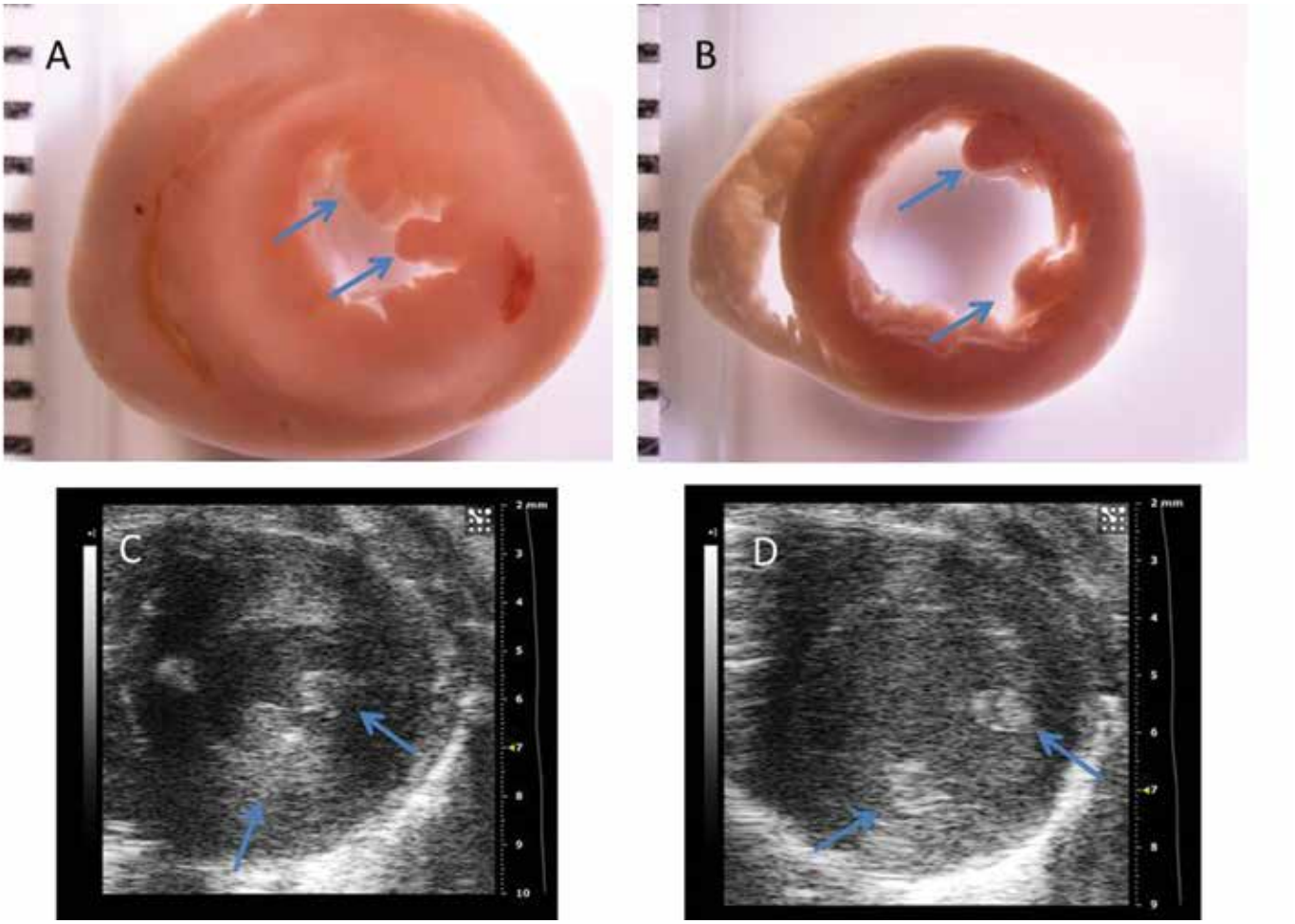


**Figure 3.** Representative cross-sectional images of cardiac gross pathology (A and B) and (2D echocardiography images (C and D). In (A and C) ErbB2$^{tg}$ mice and (B and D) wild-type mice. Blue arrows denote papillary muscles. These images illustrate the concentric left-ventricular hypertrophy and papillary muscle hypertrophy in ErbB2 mice.

umes were reduced both at end-diastole (29 ± 8 µL compared with 42 ± 7 µL, $P = 0.0001$) and end-systole (5 ± 2 µL compared with 16 ± 5 µL, $P < 0.0001$). The short-axis diastolic diameter was the same (3.4 ± 0.4 µL compared with 3.6 ± 0.3 µL, $P = 0.19$), whereas the systolic diameter was reduced in the ErbB2$^{tg}$ compared with wild-type mice (1.8 ± 0.5 µL compared with 2.2 ± 0.3 µL, $P = 0.01$). Speckle-tracking echocardiography showed reduced radial function in the ErbB2$^{tg}$ mice, with reduction in both systolic radial strain and systolic radial strain rate. However, we found no marked difference in longitudinal or circumferential systolic function in the ErbB2$^{tg}$ mice, with the systolic circumferential strain rate being higher in ErbB2$^{tg}$ mice compared with wild-type controls, but systolic circumferential strain, systolic longitudinal strain, and systolic longitudinal strain rate were all similar between genotypes. Systolic function evaluated by TDI showed no difference in systolic velocity between the 2 groups.

**Diastolic function.** ErbB2$^{tg}$ mice showed diastolic dysfunction, according to multiple Doppler parameters (Table 1, Figure 4) . The E:A ratio was inversed and lower in the ErbB2$^{tg}$ mice compared with their wild-type littermates and was combined with a prolonged deceleration time, indicating diastolic dysfunction. As a marker of relaxation and diastolic dysfunction, e' was lower and E/e' ratio elevated in ErbB2$^{tg}$ compared with wild-type mice. At baseline, 4 mice, all from the ErbB2$^{tg}$ group, had fused E and A waves. When evaluating diastolic deformation parameters from speckle tracking, we found impaired diastolic radial strain rate in ErbB2$^{tg}$ mice, but no difference in diastolic circumferential strain rate or diastolic longitudinal strain rate between groups.

**LV obstruction.** All of the ErbB2$^{tg}$ mice evaluated showed obstruction, according to color Doppler imaging, in the midpart of the LV (Figure 5) . The obstruction was caused by contact between the septum and the hypertrophied papillary muscles (Figure 5). As a consequence, the LV gradients were elevated in the ErbB2$^{tg}$ compared with wild-type mice (30.2 ± 19.1 mmHg compared with 1.8 ± 1.4 mmHg, $P < 0.0001$).The shape of the LV outflow curve, which showed a slow increase of pressure and a late peak, indicates dynamic obstruction (Figure 6) . The aortic valve was normal in all mice.

**Intraobserver variability.** Intraobserver variability (relative mean ± 1 SD) was assessed for several parameters by a single echocardiographer (HL): LVIDD, 2% ± 7%; LV internal systolic diameter, 6% ± 10%; LV anterior wall thickness, 0.6% ± 2%; LVPW, 0.9% ± 3%; LV ejection fraction, 1% ± 2%; E:A ratio, 0.0% ± 1%; e', 2% ± 2%; and LV outflow gradient, 0.5% ± 2%.

**Table 1.** Comparison of systolic and diastolic parameters (mean ± 1SD) in ErbB2$^{tg}$ mice and littermate controls

| | Control ($n$ = 17) | ErbB2$^{tg}$ ($n$ = 16) | $P$ ($t$ test) |
|---|---|---|---|
| Systolic parameters | | | |
| Ejection fraction (%) | 62 ± 7 | 81 ± 6 | <0.0001 |
| Systolic tissue velocity (mm/s) | 27 ± 3 | 26 ± 4 | 0.32 |
| Circumferential strain (%) | −26 ± 4 | −29 ± 5 | 0.14 |
| Circumferential strain rate (1/s) | −12.6 ± 2.4 | −16.3 ± 5.0 | 0.02 |
| Radial strain (%) | 40 ± 11 | 22 ± 4 | <0.0001 |
| Radial strain rate (1/s) | 12.4 ± 2.6 | 8 ± 2 | <0.0001 |
| Longitudinal strain (%) | −19 ± 3 ($n$ = 6) | −16 ± 3 ($n$ = 5) | 0.11 |
| Longitudinal strain rate (1/s) | −6.7 ± 1.2 ($n$ = 6) | −7.6 ± 2.7 ($n$ = 5) | 0.50 |
| Diastolic parameters | | | |
| E:A wave ratio | 1.4 ± 0.2 | 1.0 ± 0.2 | 0.0001 |
| Deceleration time (ms) | 24 ± 4 | 36 ± 9 | 0.0007 |
| Early-diastolic tissue velocity (e'; mm/s) | 30 ± 4 | 12 ± 4 | <0.0001 |
| E:e' wave ratio | 24 ± 4 | 65 ± 20 | <0.0001 |
| Circumferential strain rate (1/s) | 13.8 ± 2.9 | 15.6 ± 6.7 | 0.34 |
| Radial strain rate (1/s) | −15.0 ± 3.3 | −7.0 ± 1.7 | <0.0001 |
| Longitudinal strain rate (1/s) | 11.1 ± 2.4 ($n$ = 6) | 8.9 ± 2.2 ($n$ = 5) | 0.15 |

## Discussion

We found that the phenotype of the ErbB2$^{tg}$ mouse model is characterized by marked LV hypertrophy, diastolic dysfunction, and midventricular obstruction with elevated LV pressure gradients. Because all of these features are compatible with midventricular HCM in humans, we propose that ErbB2$^{tg}$ mice are an animal model of midventricular obstructive HCM. For comparison, we include images of a typical human patient with midventricular obstructive HCM (Figure 1). The morphology, pathophysiology, and hemodynamics of ErbB2$^{tg}$ mice (Figures 2 through 6) are strikingly similar to those of the human patient (Figure 1).

None of the existing murine HCM models displays this particular phenotype. At present, ErbB2 has not been reported to be associated with HCM in humans, yet this absence could be due to the fact that ErbB2 pathway remains understudied and is not represented in gene panels screened in HCM patients. This mouse model predicts that the ErbB2 or its downstream pathway proteins may be important in HCM and therefore should be evaluated in patients. In addition, the ErbB2 mouse model could be used for evaluating potential treatments for HCM. At present, no available mouse model with LV obstruction and hypertrophy is more phenotypically similar to human HCM than is the ErbB2$^{tg}$ mouse model.

In general, the life span of ErbB2$^{tg}$ mice is similar to wild type littermates, except ErbB2$^{tg}$ female mice in breeding pairs have died in late pregnancy and thus are not routinely used. Consequently, ErbB2$^{tg}$ males are breed to wild type female mice. Similarly, pregnant women with HCM and elevated gradients would be considered high risk for complications.[9] ErbB2$^{tg}$ mice are also sensitive to β-adrenergic stress due to arrhythmias.[30] Likewise, HCM in humans is also linked to arrhythmias and the most common cause of sudden death in athletes due to arrhythmias.[9]

As shown in our previous study, the ErbB2$^{tg}$ mouse has histologic and electrocardiographic features of HCM.[28-30,33] In the current study, we sought to better characterize the physiologic consequences of the previously described pathology of these mice. We confirmed our hypothesis that the ErbB2$^{tg}$ mice indeed also have many morphologic and functional features of HCM. ErbB2$^{tg}$ mice have massive LV hypertrophy compared with wild type mice, the distribution of the hypertrophy is global and involving both the anterior, septal, posterior wall and the papillary muscles. Although septal hypertrophy is typical in human HCM, a more diffuse hypertrophy is also common.[16] Hypertrophy of the papillary muscle, although not always appreciated, is a feature also seen in human HCM and especially an important cause of midcavity obstruction.[7]

In contrast to other HCM mouse models, we find LV obstruction with dynamic obstruction in ErbB2$^{tg}$ mice, a key feature of human HCM.[17] In our model, the hypertrophied papillary muscles and the septum are the main causes of the LV obstruction located in the mid part of the ventricle, where the papillary muscle is larger. This pathophysiology of midventricular obstruction is also seen in humans as illustrated in Figure 1. However, in humans the most common cause of LV obstruction is systolic anterior movement of the mitral valve, but in a substantial subset of patients, papillary muscle hypertrophy contributes to the obstruction.[7,13] In the patients with midventricular obstruction, hypertrophy of the papillary muscle is often the main cause of the left ventricle obstruction.[7]

ErbB2$^{tg}$ mice show diastolic dysfunction, as evaluated by using the conventional diastolic Doppler parameters of E:A ratio, deceleration time, e', and E:e' ratio.[3,26] In mice, a reduced E:A ratio and reduced e' are linked to diastolic dysfunction.[26] In humans, a reduced E:A ratio and prolonged deceleration time indicate impaired relaxation, whereas an increased E:e' ratio is a surrogate marker of increased LV filling pressure. According to human guidelines for grading diastolic dysfunction, ErbB2$^{tg}$ mice demonstrate moderate diastolic dysfunction.[22,25]

Interestingly, low e', which is used as a predictor of preclinical HCM in humans and typically is reduced in overt human HCM, is significantly reduced in ErbB2$^{tg}$ mice as well.[10] The cause of the diastolic dysfunction in the ErbB2$^{tg}$ mice is probably their significant myocyte disarray which, contrary to their fibrosis, is present at an early age.[30] Specifically the mice evaluated in the current study were young (less than 2 mo) and had marked myocyte dis-

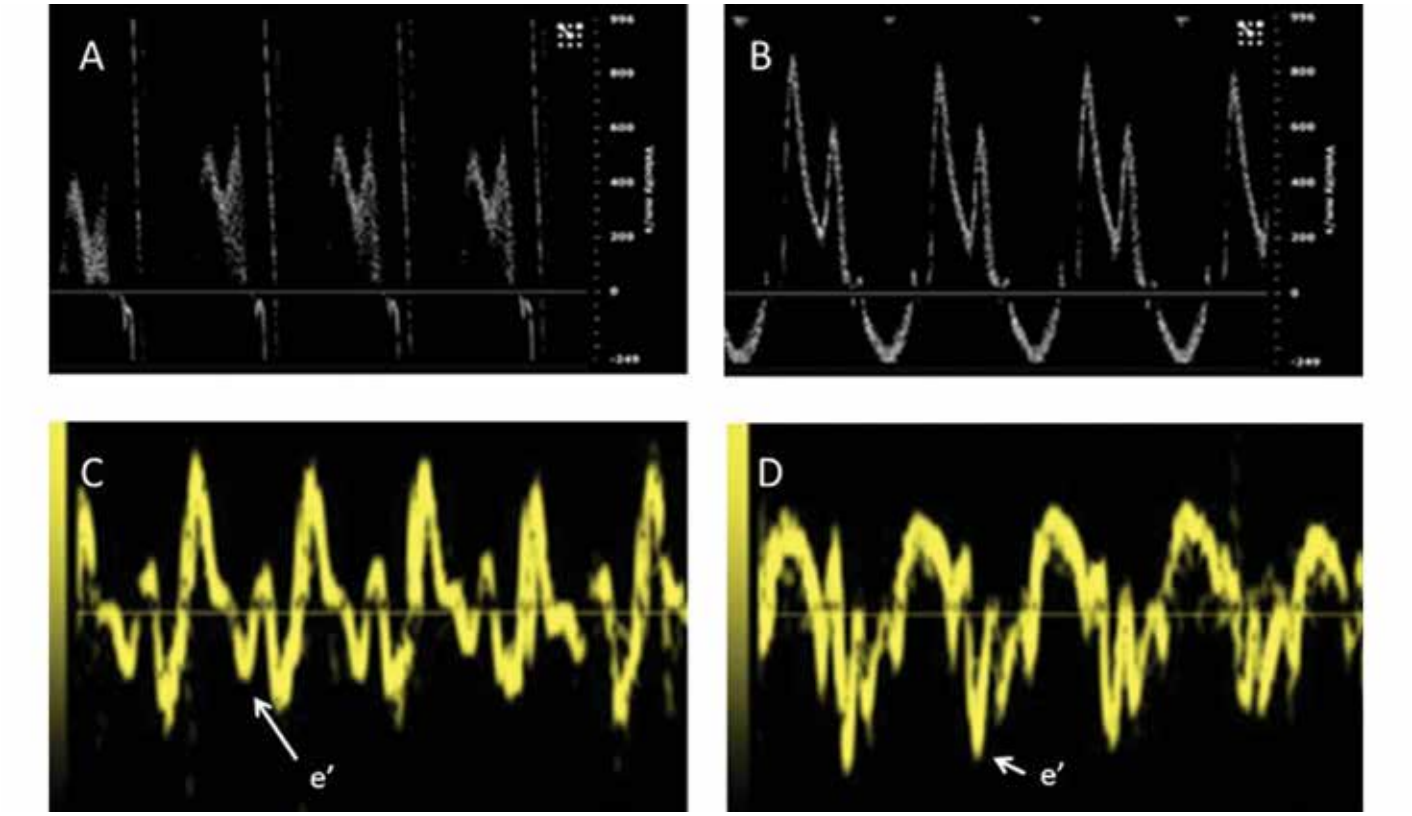


**Figure 4.** ErbB2$^{tg}$ mice show impaired relaxation and elevated filling pressure. Transmitral inflow patterns in (A) ErbB2$^{tg}$ and (B) wild-type mice. The ErbB2$^{tg}$ mouse shows a reduced E:A ratio of 1 and prolonged deceleration time, compared with the wild-type mouse. Mitral annular TDI images of (C) ErbB2$^{tg}$ and (D) wild-type mice. The ErbB2$^{tg}$ mouse shows a reduced e′ and consequently an increased E:e′ ratio, compared with the wild-type mouse.

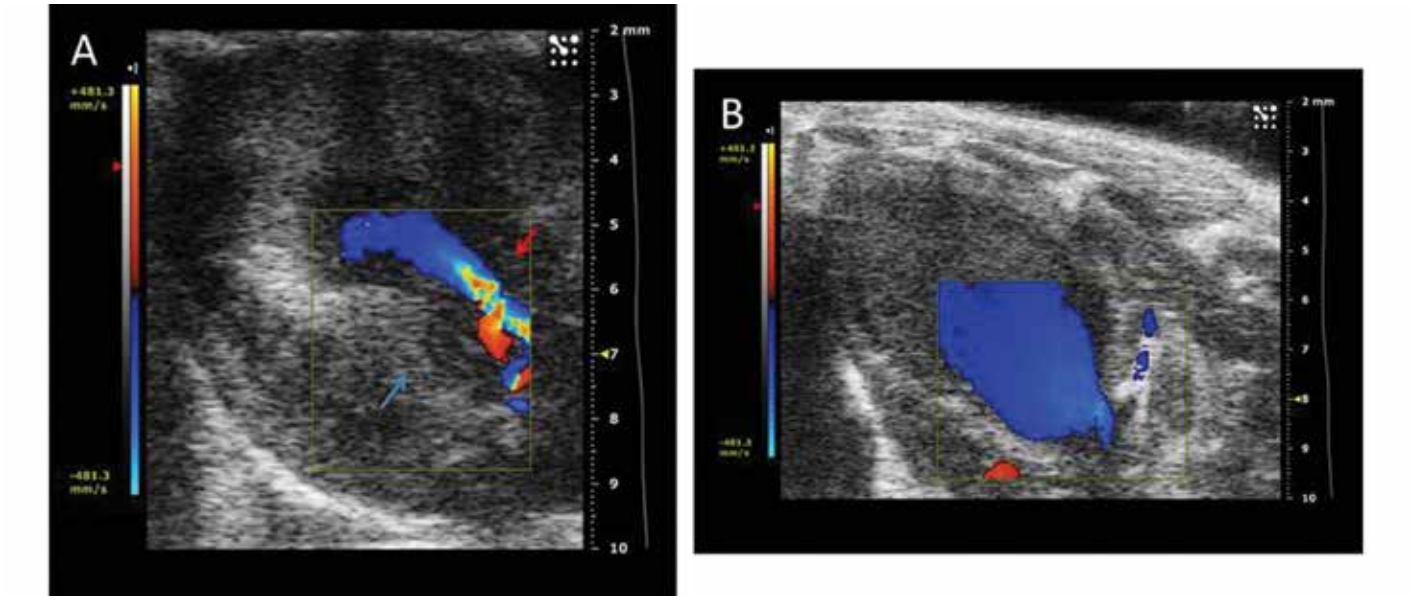


**Figure 5.** Color Doppler images of the left ventricle. (A) Left ventricular obstruction in an ErbB2$^{tg}$ mouse at the midventricular level, caused by the hypertrophied septum (red arrow) and papillary muscle (blue arrow). (B) The color Doppler image of the left ventricle of a wild-type mouse shows no obstruction.

array but little fibrosis. This same pattern is common in human HCM, especially in children and adolescents.[20,23]

When evaluating diastolic parameters derived from speckle tracking, we noted significantly impaired radial diastolic function in ErbB2$^{tg}$ mice but no marked changes in longitudinal and circumferential diastolic function. The difference in diastolic longitudinal strain rate between speckle tracking and Doppler measurements might be due to the small sample size.

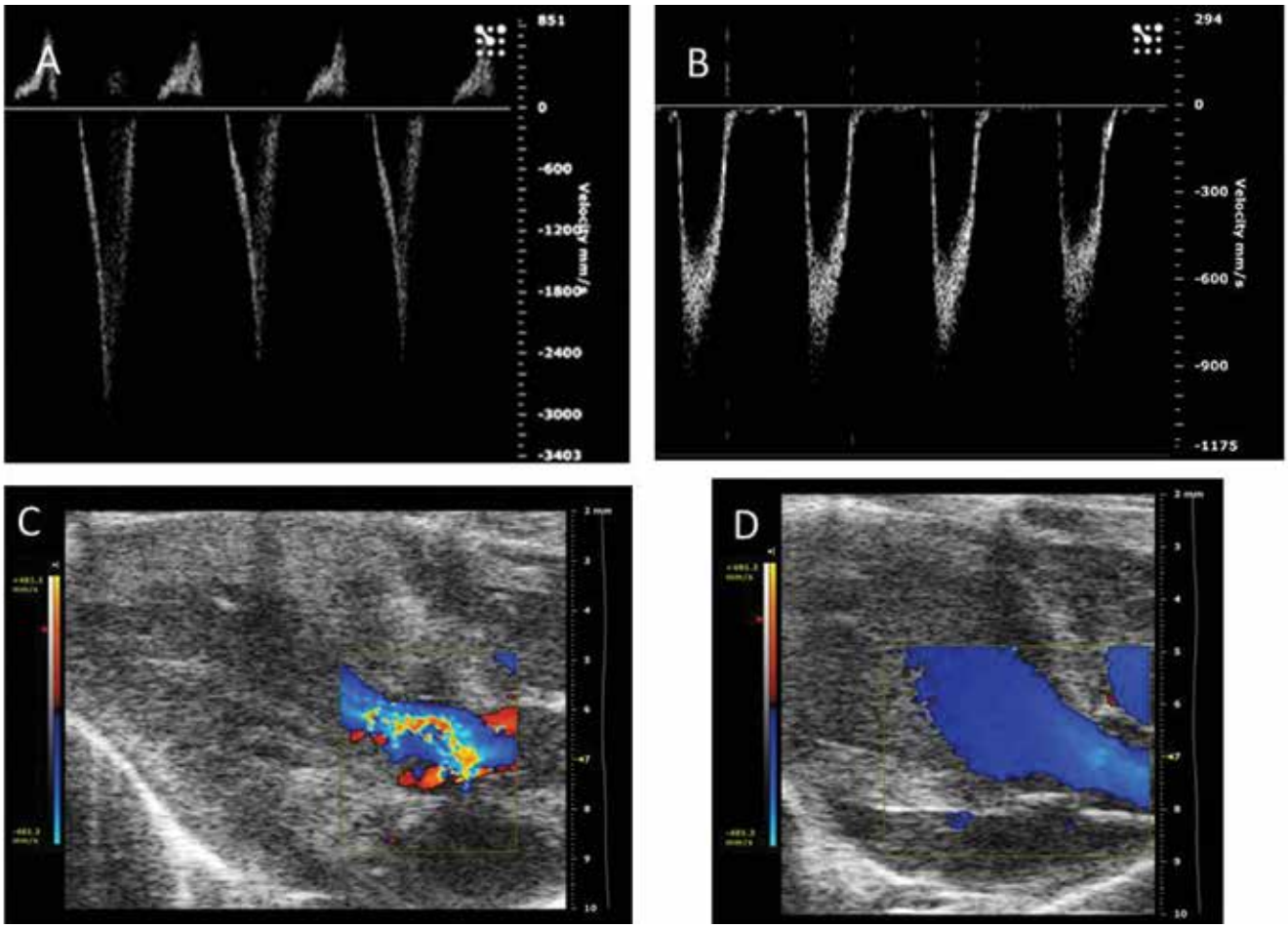


**Figure 6.** ErbB2$^{tg}$ mice have elevated left ventricular outflow tract (LVOT) gradients, indicating dynamic outflow obstruction. Pulse-wave Doppler measurement of the LVOT in (A) an ErbB2$^{tg}$ mouse and (B) wild-type mouse. Color Doppler image of the LVOT in (C) an ErbB2$^{tg}$ mouse and (D) a wild-type mouse. Notice the increased velocity (approximately 3-fold) and the dynamic LVOT obstruction (indicated by the later peak and a slower increase in velocity in the flow profile) in the ErbB2$^{tg}$ mouse compared with the wild-type mouse. The color Doppler images highlight the turbulent flow and site of the left ventricular obstruction in the ErbB2$^{tg}$ mouse.

Alternatively the difference may reflect a technical issue, given that diastolic strain rate, because of the shape of the curve, is prone to errors related to frame rate. All in all, none of the parameters derived from speckle tracking are as well validated in the evaluation of diastolic dysfunction as are the Doppler parameters.[22]

ErbB2$^{tg}$ mice have increased ejection fraction, a common feature of human HCM and mostly a consequence of decreased LV volume, which is also the case in our mouse model.[3] In our study, we noted reduced LV volumes with planimetry of the ventricle in the long axis orientation but a preserved diastolic diameter in short axis. These results suggest a decreased LV length, likely because of widespread hypertrophy including apical hypertrophy. In the current work, as a novel method of analysis of HCM in a mouse model, we used speckle tracking and TDI to characterize the systolic myocardial function in the ErbB2$^{tg}$ mice. We found significantly reduced systolic radial function in the ErbB2$^{tg}$ mice but no marked differences between groups in longitudinal or circumferential function. The strain pattern seen in human HCM is typically preserved or increased circumferential function, combined with reduced radial and longitudinal function.[6,27] The lack of a similar difference in longitudinal function in our ErbB2$^{tg}$ mice may reflect the small sample size, because a tendency toward reduced systolic longitudinal strain is apparent.

Currently no known mutations in the *ErbB2* gene result in HCM in humans. Most likely, the *ErbB2* gene has not been specifically evaluated in cases with unknown mutations. However, approximately 50% of patients with HCM have an unknown genetic cause underlying their disease.[9] Some mutations in nonsarcomeric proteins result in HCM-like phenotypes, such as seen in Fabry disease and other lysosomal storage diseases.[21] In addition, the phenotypical manifestations among family members with the same HCM-causing mutation can vary dramatically, suggesting that other factors or modifier genes influence the development of the disease.[8,15] Therefore, signaling through the ErbB2 pathway might have a modifying or triggering role in the pathogenesis of HCM and should be investigated in human HCM, especially in cases with midventricular obstruction.

Regarding limitations of the model, the feasibility of longitudinal strain analysis in ErbB2 mice is low, because the hypertrophied heart typically is displaced to the right, thus enhancing the shadow from the sternum. In general speckle tracking in mice is challenging, even when using a high-frequency ultrasound system, because of their high heart rate. Alternative, invasive means,

such as sonomicrometry and pressure–volume loop measurement, were not available to us but might be valuable in future studies.

In conclusion, we here have described a novel mouse model that displays profound LV hypertrophy, diastolic dysfunction, and midventricular obstruction with high pressure gradients. The ErbB2$^{tg}$ mouse model shows distinct morphologic HCM features compatible with midventricular obstructive HCM in humans. These characteristics make the ErbB2$^{tg}$ mouse model suitable for research on the hemodynamics and treatment of diastolic dysfunction and midventricular obstruction in HCM. The role of ErbB2 signaling in the development of HCM and midcavity obstruction is a research area that currently is not being explored. Myectomy samples from patients with midventricular obstruction should be analyzed to investigate a link between ErbB2 signaling and development of papillary muscle hypertrophy and midcavity obstruction.

## Acknowledgments

KL Gabrielson was supported by NIG grant RO1 HL088649. Lars L Sorensen is supported in part by a grant from the Ingenor August Wedell Erichsens legat, Snedkermester Sophus Jacobsen og Hustru Fund and Direktor Jacob Madsen and Olga Madsen Fund.

All authors report no conflicts of interests.

## References

1. **Abraham TP, Dimaano VL, Liang HY.** 2007. Role of tissue Doppler and strain echocardiography in current clinical practice. Circulation **116:**2597–2609.
2. **Abraham TP, Jones M, Kazmierczak K, Liang HY, Pinheiro AC, Wagg CS, Lopaschuk GD, Szczesna-Cordary D.** 2009. Diastolic dysfunction in familial hypertrophic cardiomyopathy transgenic model mice. Cardiovasc Res **82:**84–92.
3. **Afonso LC, Bernal J, Bax JJ, Abraham TP.** 2008. Echocardiography in hypertrophic cardiomyopathy: the role of conventional and emerging technologies. JACC Cardiovasc Imaging **1:**787–800.
4. **Andrews TG, Lindsey ML, Lange RA, Aune GJ.** 2013. Cardiac assessment in pediatric mice: strain analysis as a diagnostic measurement. Echocardiography **31:**375–384.
5. **Bland JM, Altman DG.** 1986. Statistical methods for assessing agreement between 2 methods of clinical measurement. Lancet **327:**307–310.
6. **Carasso S, Yang H, Woo A, Vannan MA, Jamorski M, Wigle ED, Rakowski H.** 2008. Systolic myocardial mechanics in hypertrophic cardiomyopathy: novel concepts and implications for clinical status. J Am Soc Echocardiogr **21:**675–683.
7. **de Gregorio C.** 2007. Left ventricular dynamic obstruction by atypical papillary muscle morphology: is this finding so unusual in clinical practice? J Am Soc Echocardiogr **20:**100–101.
8. **Frey N, Luedde M, Katus HA.** 2011. Mechanisms of disease: hypertrophic cardiomyopathy. Nat Rev Cardiol **9:**91–100.
9. **Gersh BJ, Maron BJ, Bonow RO, Dearani JA, Fifer MA, Link MS, Naidu SS, Nishimura RA, Ommen SR, Rakowski H, Seidman CE, Towbin JA, Udelson JE, Yancy CW.** 2011. ACCF/AHA guideline for the diagnosis and treatment of hypertrophic cardiomyopathy: Executive summary: a report of the American College of Cardiology Foundation/American Heart Association Task Force on practice guidelines. Circulation.**124:**2761–2796.
10. **Ho CY, Sweitzer NK, McDonough B, Maron BJ, Casey SA, Seidman JG, Seidman CE, Solomon SD.** 2002. Assessment of diastolic function with Doppler tissue imaging to predict genotype in preclinical hypertrophic cardiomyopathy. Circulation **105:**2992–2997.
11. **Institute for Laboratory Animal Research.** 2011. Guide for the care and use of laboratory animals, 8th ed. Washington (DC): National Academies Press.
12. **Kazmierczak K, Muthu P, Huang W, Jones M, Wang Y, Szczesna-Cordary D.** 2012. Myosin regulatory light chain mutation found in hypertrophic cardiomyopathy patients increases isometric force production in transgenic mice. Biochem J **442:**95–103.
13. **Klues HG, Roberts WC, Maron BJ.** 1991. Anomalous insertion of papillary muscle directly into anterior mitral leaflet in hypertrophic cardiomyopathy. Significance in producing left ventricular outflow obstruction. Circulation **84:**1188–1197.
14. **Konstandin MH, Toko H, Gastelum GM, Quijada P, De La Torre A, Quintana M, Collins B, Din S, Avitabile D, Volkers M, Gude N, Fassler R, Sussman MA.** 2013. Fibronectin is essential for reparative cardiac progenitor cell response after myocardial infarction. Circ Res **113:**115–125.
15. **Marian AJ, Roberts R.** 2001. The molecular genetic basis for hypertrophic cardiomyopathy. J Mol Cell Cardiol **33:**655–670.
16. **Maron MS, Maron BJ, Harrigan C, Buros J, Gibson CM, Olivotto I, Biller L, Lesser JR, Udelson JE, Manning WJ, Appelbaum E.** 2009. Hypertrophic cardiomyopathy phenotype revisited after 50 y with cardiovascular magnetic resonance. J Am Coll Cardiol **54:**220–228.
17. **Maron MS, Olivotto I, Zenovich AG, Link MS, Pandian NG, Kuvin JT, Nistri S, Cecchi F, Udelson JE, Maron BJ.** 2006. Hypertrophic cardiomyopathy is predominantly a disease of left ventricular outflow tract obstruction. Circulation **114:**2232–2239.
18. **Matsubara K, Nakamura T, Kuribayashi T, Azuma A, Nakagawa M.** 2003. Sustained cavity obliteration and apical aneurysm formation in apical hypertrophic cardiomyopathy. J Am Coll Cardiol **42:**288–295.
19. **McConnell BK, Fatkin D, Semsarian C, Jones KA, Georgakopoulos D, Maguire CT, Healey MJ, Mudd JO, Moskowitz IP, Conner DA, Giewat M, Wakimoto H, Berul CI, Schoen FJ, Kass DA, Seidman CE, Seidman JG.** 2001. Comparison of 2 murine models of familial hypertrophic cardiomyopathy. Circ Res **88:**383–389.
20. **Menon SC, Eidem BW, Dearani JA, Ommen SR, Ackerman MJ, Miller D.** 2009. Diastolic dysfunction and its histopathologic correlation in obstructive hypertrophic cardiomyopathy in children and adolescents. J Am Soc Echocardiogr **22:**1327–1334.
21. **Monserrat L, Gimeno-Blanes JR, Marin F, Hermida-Prieto M, Garcia-Honrubia A, Perez I, Fernandez X, de Nicolas R, de la Morena G, Paya E, Yague J, Egido J.** 2007. Prevalence of fabry disease in a cohort of 508 unrelated patients with hypertrophic cardiomyopathy. J Am Coll Cardiol **50:**2399–2403.
22. **Nagueh SF, Appleton CP, Gillebert TC, Marino PN, Oh JK, Smiseth OA, Waggoner AD, Flachskampf FA, Pellikka PA, Evangelista A.** 2009. Recommendations for the evaluation of left ventricular diastolic function by echocardiography. J Am Soc Echocardiogr **22:**107–133.
23. **Ohsato K, Shimizu M, Sugihara N, Konishi K, Takeda R.** 1992. Histopathologic factors related to diastolic function in myocardial hypertrophy. Jpn Circ J **56:**325–333.
24. **Ram R, Mickelsen DM, Theodoropoulos C, Blaxall BC.** 2011. New approaches in small animal echocardiography: imaging the sounds of silence. Am J Physiol Heart Circ Physiol **301:**H1765–H1780.
25. **Redfield MM, Jacobsen SJ, Burnett JC Jr, Mahoney DW, Bailey KR, Rodeheffer RJ.** 2003. Burden of systolic and diastolic ventricular dysfunction in the community: appreciating the scope of the heart failure epidemic. JAMA **289:**194–202.
26. **Schaefer A, Klein G, Brand B, Lippolt P, Drexler H, Meyer GP.** 2003. Evaluation of left ventricular diastolic function by pulsed Doppler tissue imaging in mice. J Am Soc Echocardiogr **16:**1144–1149.
27. **Serri K, Reant P, Lafitte M, Berhouet M, Le Bouffos V, Roudaut R, Lafitte S.** 2006. Global and regional myocardial function quantification by 2-dimensional strain: application in hypertrophic cardiomyopathy. J Am Coll Cardiol **47:**1175–1181.
28. **St John Sutton MG, Lie JT, Anderson KR, O'Brien PC, Frye RL.** 1980. Histopathologic specificity of hypertrophic obstructive cardiomyopathy. Myocardial fibre disarray and myocardial fibrosis. Br Heart J **44:**433–443.
29. **Sysa-Shah P, Sorensen LL, Abraham MR, Gabrielson KL.** 2015. Electrocardiographic characterization of cardiac hypertrophy in

mice that overexpress the ErbB2 receptor tyrosine kinase. Comp Med **65:**295–307.

30. **Sysa-Shah P, Xu Y, Guo X, Belmonte F, Kang B, Bedja D, Pin S, Tsuchiya N, Gabrielson K.** 2012. Cardiac-specific over-expression of epidermal growth factor receptor 2 (ErbB2) induces pro-survival pathways and hypertrophic cardiomyopathy in mice. PLoS One **7:**e42805.
31. **Tanaka N, Dalton N, Mao L, Rockman HA, Peterson KL, Gottshall KR, Hunter JJ, Chien KR, Ross J Jr.** 1996. Transthoracic echocardiography in models of cardiac disease in the mouse. Circulation **94:**1109–1117.
32. **Tardiff JC, Hewett TE, Palmer BM, Olsson C, Factor SM, Moore RL, Robbins J, Leinwand LA.** 1999. Cardiac troponin T mutations result in allele-specific phenotypes in a mouse model for hypertrophic cardiomyopathy. J Clin Invest **104:**469–481.
33. **Varnava AM, Elliott PM, Sharma S, McKenna WJ, Davies MJ.** 2000. Hypertrophic cardiomyopathy: the interrelation of disarray, fibrosis, and small vessel disease. Heart **84:**476–482.
34. **Yuan L, Wang T, Liu F, Cohen ED, Patel VV.** 2010. An evaluation of transmitral and pulmonary venous Doppler indices for assessing murine left ventricular diastolic function. J Am Soc Echocardiogr **23:**887–897.